

RESEARCH ARTICLE

Response of the copepod *Acartia tonsa* to the hydrodynamic cues of small-scale, dissipative eddies in turbulence

Dorsa Elmi¹, Donald R. Webster^{1,*} and David M. Fields²

ABSTRACT

This study quantifies the behavioral response of a marine copepod (*Acartia tonsa*) to individual, small-scale, dissipative vortices that are ubiquitous in turbulence. Vortex structures were created in the laboratory using a physical model of a Burgers vortex with characteristics corresponding to typical dissipative vortices that copepods are likely to encounter in the turbulent cascade. To examine the directional response of copepods, vortices were generated with the vortex axis aligned in either the horizontal or vertical direction. Tomographic particle image velocimetry was used to measure the volumetric velocity field of the vortex. Three-dimensional copepod trajectories were digitally reconstructed and overlaid on the vortex flow field to quantify *A. tonsa*'s swimming kinematics relative to the velocity field and to provide insight into the copepod behavioral response to hydrodynamic cues. The data show significant changes in swimming kinematics and an increase in relative swimming velocity and hop frequency with increasing vortex strength. Furthermore, in moderate-to-strong vortices, *A. tonsa* moved at elevated speed in the same direction as the swirling flow and followed spiral trajectories around the vortex, which would retain the copepod within the feature and increase encounter rates with other similarly behaving *Acartia*. While changes in swimming kinematics depended on vortex intensity, orientation of the vortex axis showed minimal significant effect. Hop and escape jump densities were largest in the vortex core, which is spatially coincident with the peak in vorticity, suggesting that vorticity is the hydrodynamic cue that evokes these behaviors.

KEY WORDS: Marine zooplankton, Fluid–organism interactions, Behavior response, Burgers vortex

INTRODUCTION

Microscale turbulence is an important driving force in the structure and function of zooplankton communities. Turbulent processes have been shown to alter metabolic rate, predator–prey encounter rate, grazing rate, egg production, swimming behavior and population dynamics of marine zooplankton (Alcaraz and Saiz, 1992; Saiz et al., 1992; Saiz and Alcaraz, 1992a,b; Saiz and Kiørboe, 1995; Fields and Yen, 1997). Another key aspect of ocean turbulence is its influence on the vertical distribution of copepods in response to turbulence intensity within the water column (Heath et al., 1988; Haurv et al., 1990; Mackas et al., 1993; Lagadeuc et al., 1997; Incze et al., 2001; Visser et al., 2001; Manning and Bucklin, 2005). Ocean turbulence

intensity (typically quantified as energy dissipation rate) varies in time and space. Turbulence decreases exponentially with depth, giving rise to larger and larger eddies with increasing depth. Turbulent dissipation rate in the surface ocean can be 5–6 orders of magnitude larger than that found in deeper waters. Similarly, different regions of the ocean can have significantly different turbulence levels. Coastal regions and tidally swept areas can have 3–5 orders of magnitude higher turbulence levels than those in the open ocean (Granata and Dickey, 1991; Kiørboe and Saiz, 1995). Currently, there is limited understanding of the directional sensory response of copepods to the fine-scale flow structure of turbulent flows that ultimately affect the fitness of marine copepods.


At the scale of zooplankton, turbulent flows present a rich flow structure that may provide critical hydrodynamic sensory cues. Computer simulations and experiments reveal that coherent vortical structures develop in turbulent flow (e.g. Vincent and Meneguzzi, 1991). These small worm-like eddies are similar in size to the Kolmogorov scales (0.2–6 mm diameter) and are oriented in random directions. Yamazaki (1993) suggested that these organized flow structures act as aggregating mechanisms where swimming copepods form patches that can increase encounter rates with conspecifics and foster predation rates by predators.

Copepods rely on their sensory hairs, called setae, to detect hydrodynamic signals. The sensitivity of copepods to hydrodynamic signals depends on bending and deflection of their setae. Yen et al. (1992) reported that setal displacement as small as 10 nm can elicit a neurological response in copepods. However, behavioral responses often require stimulation of multiple sensors caused by a characteristic strain rate to trigger attack responses or escape jumps (Fields and Yen, 1997; Kiørboe et al., 1999). It is also apparent that the responses to hydrodynamical signals are species specific and vary by sex and developmental stage (Woodson et al., 2014). Copepods also are sensitive to the direction of the hydrodynamic signals, are able to escape the flow disturbance of a nearby predator (Fields and Yen, 1997; Fields, 2010; Takagi and Hartline, 2018) and attack the flow created by potential prey (Fields and Yen, 2002; Browman et al., 2011). It is largely unknown whether there is a directional response of copepods to small-scale turbulent eddies, although Webster et al. (2015) observed that *Acartia tonsa* significantly altered their swimming behavior in the small-scale Burgers vortex of a certain strength.

This study hypothesized that copepods detect and respond to hydrodynamic signals associated with dissipative eddies of the turbulent cascade at specific thresholds by changing their swimming behaviors, including changing their swimming path, swimming velocity, turning frequency, trajectory orientation, and jump orientation and strength. Given the chaotic changes of the velocity field in turbulent flows, observation of copepod interaction with turbulent eddies and making accurate measurements of their swimming kinematics is a challenging problem. Therefore, in order to improve our mechanistic understanding of copepod responses, this

¹School of Civil and Environmental Engineering, Georgia Institute of Technology, Atlanta, GA 30332-0355, USA. ²Bigelow Laboratory for Ocean Sciences, East Boothbay, ME 04544, USA.

*Author for correspondence (dwebster@ce.gatech.edu)

 D.R.W., 0000-0002-3397-9222

List of symbols and abbreviations

a	axial (extensional) strain rate parameter
A	area
$e_{r\theta}$	shear component of strain rate
e_{xx}	axial component of strain rate
NGDR	net-to-gross displacement ratio
PIV	particle image velocimetry
PRT	proportional residence time in the vortex core
r_B	radius of the vortex
(r, θ, x)	cylindrical polar coordinate system
u_r	radial velocity
u_{rms}	root mean square of the velocity fluctuations
u_x	axial velocity
u_θ	azimuthal velocity
Γ	total circulation
ε	turbulent dissipation rate
η	Kolmogorov length scale
ν	fluid viscosity
ω_x	axial component of vorticity

study took an alternative approach by using the Burgers vortex model, which generates a stable dissipative eddy in the laboratory (Webster and Young, 2015). The Burgers vortex is an ideal model of a turbulent eddy at viscous dissipative length scales (of the order of millimeters) (Burgers, 1948; Saffman, 1997; Jumars et al., 2009; Webster and Young, 2015). A sub-hypothesis is that the behavioral response depends on the orientation of the vortex, thereby leading to directional responses. This study generated Burgers vortex structures in horizontal and vertical orientations to examine directional responses of copepods. Understanding how small planktonic animals respond to these small-scale dissipative eddy features informs our understanding of the impact of turbulence on individual animals in the ocean and will help us to interpret the role of turbulence in governing the biogeography of zooplankton species.

MATERIALS AND METHODS

Burgers vortex

Oceanic turbulence forms vortex tubes of the order of the Kolmogorov length scale that last for a few seconds (Vincent and Meneguzzi, 1991). Stretching of the vortex tube is a fundamental component of these natural vortex structures as they approach the Kolmogorov length scale (η) (Davidson, 2015). The Burgers vortex is an ideal model for simulating these vortex structures (Burgers, 1948; Jumars et al., 2009). A Burgers vortex is a steady solution of the Navier–Stokes equations, which consists of fluid rotation around an axis combined with stretching along the axis. As a consequence, the Burgers vortex balances the radially outward diffusion of vorticity with the radially inward advection imposed by vortex stretching, which generates a stable vortex structure in time and space. In the current study, this allowed high-resolution imaging of the volume of interest and observations of the swimming kinematics of copepods as they interacted with the eddy feature.

In a cylindrical polar coordinate system (r, θ, x), Burgers vortex flow has axial velocity, u_x , azimuthal velocity, u_θ , and radial velocity, u_r , components. The flow field for the Burgers vortex is described by:

$$u_x = 2ax, \quad (1)$$

$$u_\theta = \frac{\Gamma}{2\pi r} (1 - e^{-r^2 a / 2\nu}), \quad (2)$$

$$u_r = -ar, \quad (3)$$

in which Γ is the total circulation, a is the axial (extensional) strain rate parameter, and ν is the fluid viscosity. For a Burgers vortex, the vorticity field consists of the axial component alone and is defined as:

$$\omega_x = \frac{\Gamma}{2\pi\nu} e^{-r^2 a / 2\nu}. \quad (4)$$

Circulation and axial strain rate are the key characteristic parameters of the vortex tube. Circulation, which represents the volumetric rotational strength of the vortex, is defined as the area (A) integral of vorticity over the vortex core:

$$\Gamma = \iint \omega_x \cdot dA. \quad (5)$$

When relating these fundamental definitions to turbulent eddies, circulation can be expressed in terms of the root mean square of the velocity fluctuations, u_{rms} , and the characteristic radius of the vortex, $r_B = \sqrt{(2\nu/a)}$ (Davidson, 2015):

$$\Gamma = 2\pi r_B u_{rms}. \quad (6)$$

As the smallest turbulent eddies dissipate by viscous effects, a good indicator of the characteristic vortex radius is the dissipation rate of kinetic energy. Jumars et al. (2009) defined $r_B = 8.1\eta$ (where η is the Kolmogorov scale) as the ‘typical’ radius of a Burgers vortex, at which one-half of the dissipation occurs at larger scales and one-half of the dissipation occurs at smaller scales. Further, Jumars et al. (2009) reported that 90% of the dissipation rate occurs within a range of vortex radius of 2.7η to 58η .

The laboratory apparatus used to generate the Burgers vortex structure has been previously described (Webster and Young, 2015), although the parameter range was larger in the current study as described below. Briefly, two coaxial disks, positioned at the center of the observation tank, rotated at the same rate. The disks induced rotating motion of the fluid in the region between them and the resulting fluid motion diffused vorticity radially outward. At the same time, water was drawn through the hollow shaft attached to the center of the disks, which stretched the vortex and advected vorticity toward the center axis. The system was designed with a number of degrees of freedom (e.g. flow rate through the shafts, disk rotation rate and disk spacing length) that could be adjusted to generate a stable vortex structure between the disks. By varying the rotation rate of the disks and the flow rate into the hollow shaft, different Burgers vortices were created with specific characteristics that targeted levels of turbulence intensity.

To examine the directional response of copepods to vortex motions, we designed two apparatuses, one that generated the Burgers vortex axis aligned in the horizontal direction and one that generated the vortex axis aligned in the vertical direction (Fig. 1). The horizontal apparatus in this study consisted of a tank ($20.6 \times 20.6 \times 27.3$ cm W×L×H) with acrylic sheet walls. The tank for the vertical apparatus was slightly larger ($25.4 \times 25.4 \times 27.9$ cm W×L×H), and in both cases the tank walls were very far away from the vortex structure. In both apparatuses, the disks (radius 1.5 cm) were located near the center of the tank, mounted on hollow stainless-steel shafts (with an inner diameter of 0.62 cm) that extended from the disks, through the acrylic tank wall, to the drive assembly. Rotation rate of the disks was controlled by a DC motor. Water flow rate through the disk holes was controlled by a flowmeter valve, which was connected with a tube to the hollow shaft. Disk rotation rate and water flow rate were monitored and maintained at a constant level during the experiments to establish a stable vortex structure.

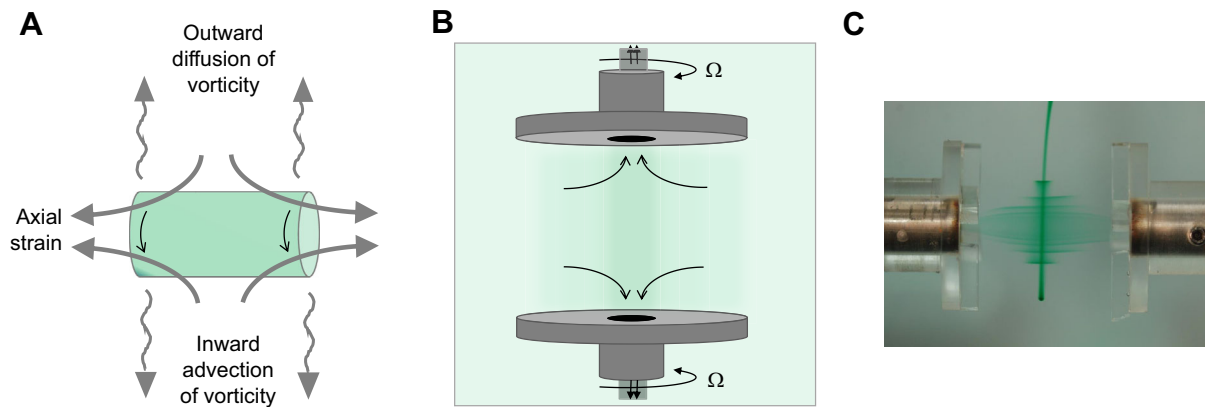


Fig. 1. Representations of the Burgers vortex. (A) Burgers vortex cartoon (horizontal treatment): outward diffusion of vorticity is balanced by inward advection of vorticity that is caused by the axial strain rate. (B) Sketch of the Burgers vortex apparatus – vertical treatment. Ω , angular velocity of the disks and shafts. (C) Dye visualization of the Burgers vortex – horizontal treatment for a level 3 vortex. The dye filament enters from above and spirals around the vortex core while being stretched toward the disk faces.

Flow measurements

Tomographic particle image velocimetry (tomographic PIV) was used to measure the three-dimensional flow field (Elsinga et al., 2006) and to confirm that it quantitatively matched the target parameters of small-scale eddies in copepod habitats. Tomographic PIV reconstructed the volumetric position of small particles suspended in the fluid that were imaged by collecting scattered laser light via four cameras simultaneously. Particle displacement was calculated via cross-correlation of particle location in consecutive volumetric reconstructions in order to measure the local three-dimensional velocity vector. Three-dimensional flow measurements were required for this flow as the local velocity vector included three components of motion and the flow field varied in three coordinate directions.

The tomographic PIV system (Murphy et al., 2012) used four high-resolution cameras (Phantom v210, 1280×800 pixels) to measure flow fields at the scale of the copepod. Images were captured digitally at a rate of 24 frames s^{-1} . To resolve the small length scales in this study, a 105 mm focal length lens (Nikon) was used for each camera. Scheimpflug mounts were used to change the orientation of the lens to correct the plane of focus on the cameras (Murphy et al., 2012). Orgasol polyamide powder (20 μm diameter; specific weight of 1.03 $g\ cm^{-3}$; Arkema group) tracked the fluid motion within the tank. An infrared laser (808 nm wavelength) illuminated the tracer particles. Experiments were performed in a dark room to eliminate any light outside the control volume that could increase the level of error in the flow measurements. The vortex volume was reconstructed in DaVis software (LaVision Inc.) using MART algorithms. Three-dimensional cross-correlation calculated the velocity field in the vortex by measuring particle displacement in consecutively reconstructed volumes (Elsinga et al., 2006).

Characterizing the Burgers vortex flow in the apparatuses

This study generated a Burgers vortex for each of four levels corresponding to turbulent dissipation rates that copepods are likely to encounter in their habitat (Webster et al., 2004). For each turbulence level, we targeted creating a vortex with $r_B=8.1\eta$, which as explained above can be considered ‘typical’ in the dissipative range of scales.

Higher vorticity and axial strain rate correspond to stronger turbulence intensity. That is, as vortex stretching increases by axial strain rate, the vortex swirl velocity increases and the core radius (r_B) gets smaller. Peak vorticity occurs at the vortex centerline (i.e. $r=0$), then decreases exponentially with the vortex radius as a result of

viscous effects (Eqn 4) (Fig. 2B). Shear strain rate, $e_{r\theta}$, is zero at the vortex centerline, increases to a peak at a radius greater than the characteristic radius of the vortex, and then decreases back to zero at large radii (Fig. 2A). Furthermore, the strongest vortex intensity (level 4) has the greatest vorticity and shear strain rate (Fig. 2A,B). The axial component of strain rate, $e_{xx}=2a$, is spatially constant and increases with vortex strength. Following this description, the Burgers vortex structure shows a core of high vorticity, which occurs within an annulus area of large values of shear strain rate. The structure of the Burgers vortex is an advantage for this study, as it spatially separates these possible hydrodynamic cues for the copepods’ behavioral responses. Locating the behavior change of copepods in the vortex volume determines the co-occurring hydrodynamic cue that likely triggers behavioral responses.

Comparing flow measurements with the target flow was the first step in studying the interaction of copepods with small-scale vortex tubes. The target parameters corresponded to turbulent dissipation rates of 0.002–0.25 $cm^2\ s^{-3}$ (Table 1), which agrees with the natural environments of the target copepod species (Webster et al., 2004). The target turbulence parameters for the present study, ϵ and η , were determined for oceanic conditions typical of coastal and surface oceanic locations. The target values of r_B , a and Γ based on these turbulence characteristics are presented in Table 1. Note that only levels 2 and 3 were produced in Webster and Young (2015) and Webster et al. (2015) and only for the horizontal arrangement, whereas the current study expanded the parameter space to examine a broad range of copepod behavior reactions. In Table 1, level 1 represents the mildest turbulence characteristics, with small velocity fluctuations and dissipation rates. As turbulence intensity increases from level 1 to 4, the length scales become smaller and axial stretching, a , and circulation, Γ , increase.

Tomographic PIV experiments were performed for four vortex intensities for both the horizontal and vertical vortex alignments. Fig. 2C,D compares an example of a measured vorticity field with the theoretical vorticity field. The axial strain rate, vorticity and circulation were calculated from the measured velocity fields and compared with the target parameters. This is an iterative process, in which disk rotation rate, flow rate through the shafts and separation distance of the disk faces were independently adjusted until the target vortex parameters were achieved. The axial strain rate parameter (a) was calculated from the slope of the axial velocity (u_x) profiles (see Eqn 1). Vortex circulation (Γ) was calculated from the

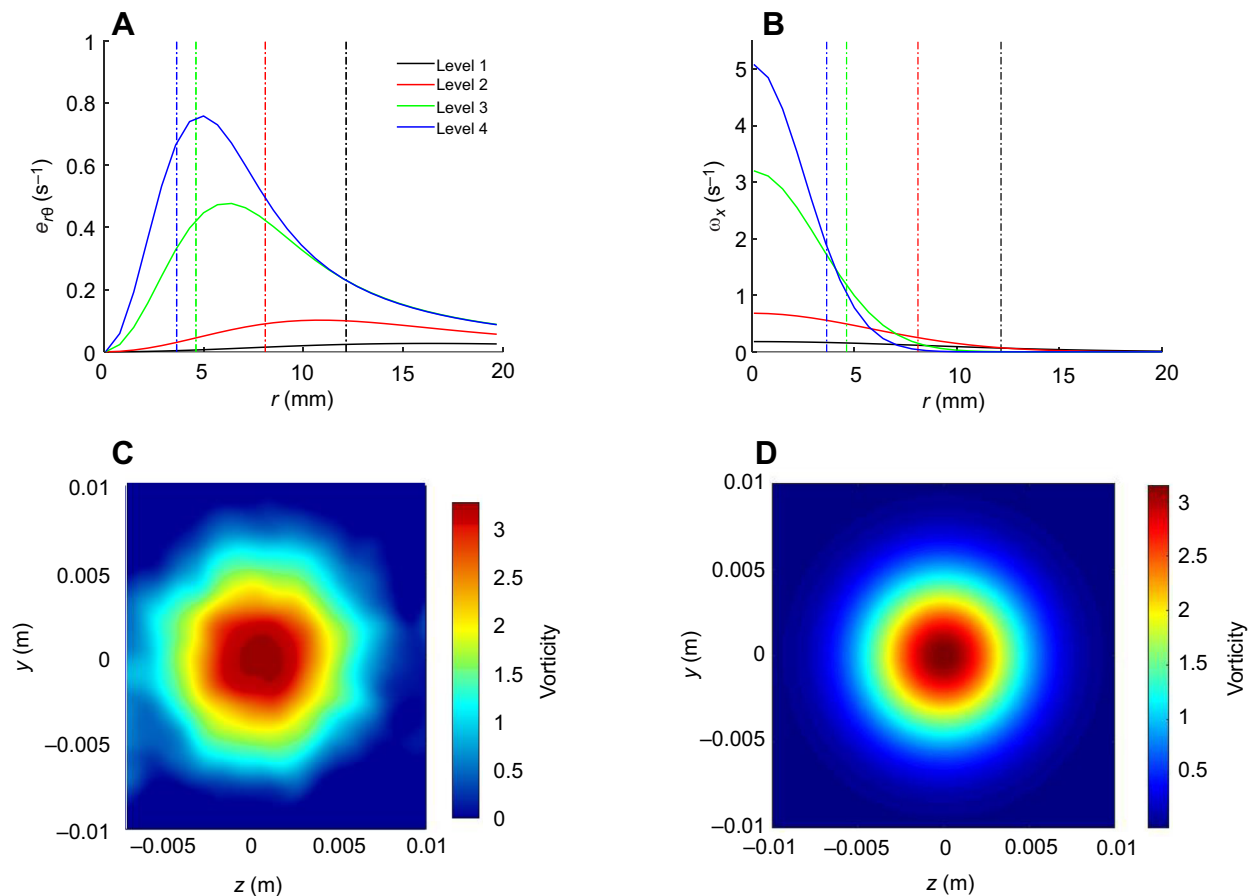


Fig. 2. Shear strain rate and vorticity. (A,B) Radial profiles of (A) shear strain rate ($e_{r\theta}$) and (B) vorticity (ω) of the Burgers vortex model for four vortex strengths, levels 1–4, which were defined by measurements in the isotropic turbulence apparatus by Webster et al. (2004). The vertical dashed line indicates the characteristic radius of the vortex (r_B), which gets smaller for increasing vortex intensity. (C,D) Contours of the axial component of vorticity (level 3, horizontal treatment; C) experimental measurements and (D) theoretical vorticity field.

vorticity field using Eqn 5. The results show good agreement between measurements and target values (Table 1). The vortex treatments were highly repeatable; hence, the flow measurements were done separately from the copepod trials.

Behavioral assay experiments

The target copepod species of this study was *Acartia tonsa* Dana 1849, which is a hop–sink swimmer and a common species of estuary ecosystems. Adult *A. tonsa* have long antennae and a body

length of 0.75–1.2 mm. Distributed all around their antennules are setal hairs that act as mechanoreceptors. *Acartia tonsa* were reared in culture at the Bigelow Laboratory for Ocean Sciences in East Boothbay, ME, USA. Populations of mixed-sex adults were shipped overnight in thermally insulated containers to the Georgia Institute of Technology in Atlanta, GA, USA. Experiments were conducted in a temperature-controlled room at 13°C and the water salinity level was maintained at 33 ppt. Digital recordings were made in a dark room to avoid behavioral responses to changes in light (e.g. Fields et al., 2012). Copepods were in the experimental tank during the whole experiment and were fed the cryptophyte *Rhodomonas salina* (10^4 – 10^5 cells ml^{-1} ; CCMP # 1319) before starting the experiments.

Video recording started at least 15 min after the Burgers vortex reached steady state. Images of free-swimming copepods in the observation volume were taken using two synchronized cameras (FLIR-FLEA 3 FL3-U3-13Y3M-C) recording at 15 frames s^{-1} . The frame rate was sufficient to quantify the movement of *A. tonsa* with displacement of only a few pixels between successive frames. Cameras were equipped with Nikon 50 mm lenses and mounted in orthogonal perspective. The field of view (~ 27 ml; $3 \times 3 \times 3$ cm) was illuminated with red diodes (630 nm), which cause no behavioral response in *A. tonsa* (Fig. 3A).

Copepod trajectories in each camera were tracked manually using the DLTdv5 package for MATLAB (Hedrick, 2008). A self-developed MATLAB code was used to match trajectories from the

Table 1. Burgers vortex parameters for each level

Vortex intensity level	1	2	3	4
Target ε ($\text{cm}^2 \text{s}^{-3}$)	0.002	0.009	0.096	0.25
Target η (cm)	0.15	0.1	0.057	0.045
Target r_B (cm)	1.21	0.81	0.46	0.36
Target a (s^{-1})	0.014	0.030	0.093	0.15
Target Γ ($\text{cm}^2 \text{s}^{-1}$)	0.84	1.41	2.15	2.13
Horizontal treatment				
Measured a (s^{-1})	0.014	0.025	0.1	0.14
Measured Γ ($\text{cm}^2 \text{s}^{-1}$)	0.92	1.70	2.52	2.45
Vertical treatment				
Measured a (s^{-1})	0.015	0.028	0.092	0.143
Measured Γ ($\text{cm}^2 \text{s}^{-1}$)	0.89	1.43	2.58	2.39

The turbulent dissipation rate, ε , and Kolmogorov length scale, η , are from Webster et al. (2004). r_B , radius of the vortex; a , axial strain rate; Γ , circulation.

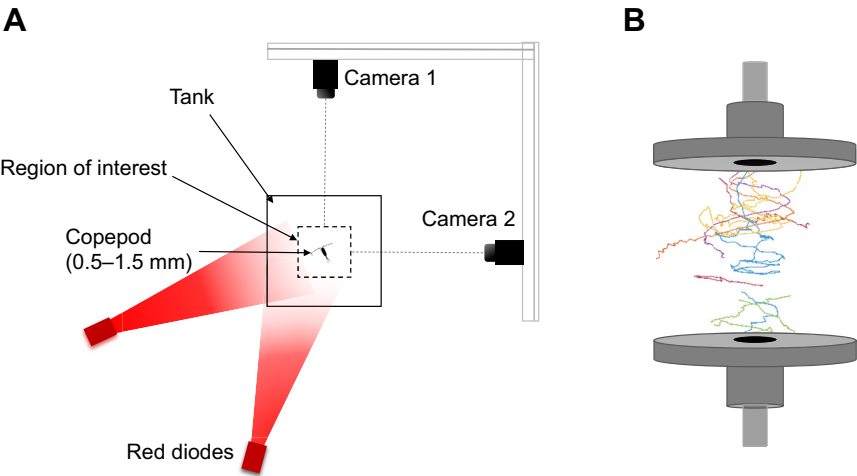


Fig. 3. Experimental setup. (A) Schematic diagram of the experimental setup during behavior assays. Cameras 1 and 2 (50 mm lenses) acquire images of the vortex volume from orthogonal perspectives, while copepods swim inside the vortex volume. (B) Representative three-dimensional copepod trajectories in the vortex volume.

two perspectives and create the three-dimensional copepod trajectories (Fig. 3B).

The three-dimensional trajectories were overlaid on the Burgers vortex flow field (measured separately as described above) to match copepod behavior to the surrounding flow conditions. Subsequent statistical analysis of the swimming trajectories quantified the behavioral responses.

Behavioral assay experiments consisted of two orientation treatments (horizontal and vertical), and for each orientation treatment there were five flow levels: control, which represents a no-flow condition or stagnant water, and four vortex intensity levels (Table 1). Experiments for each treatment were conducted with three different copepod populations. In each replicate, the flow levels were recorded in random order. For each replicate, a minimum of 22 and a maximum of 56 copepod trajectories were taken at each level (Table 2). Swimming kinematics measured in this study were: (1) relative swimming velocity, (2) turn frequency, (3) trajectory pattern [net-to-gross displacement ratio (NGDR), fractal dimension, and ratio of spiral trajectories to total number of trajectories reported as a percentage], (4) trajectory alignment relative to the vortex axis, gravity and the local flow direction (quantified as angle), (5) jump (hops and escapes) characterization (i.e. jump frequency, jump acceleration and jump density), (6) jump angle relative to the vortex axis and gravity, and (7) proportional residence time in the vortex core (PRT).

Relative swimming velocity was defined as copepod swimming velocity minus local fluid velocity. Turn frequency was calculated as the number of turns per copepod per period (s), where a turn was defined by a change in trajectory direction by more than 20 deg in the observation volume. NGDR characterizes the linearity of trajectories and was consistently calculated for trajectory segments of 20 s duration to avoid scale-dependent results (Tiselius, 1992). Large values of NGDR indicate straight, ballistic trajectories, whereas

small values indicate curved, loopy trajectories. Unlike NGDR, fractal dimension is a scale-independent metric to quantify the complexity of trajectories. The fractal dimension was calculated for each trajectory projected onto the $r-\theta$ (or $y-z$) plane to quantify the shape complexity in the plane perpendicular to the vortex axis. The calculation was performed using a box-counting algorithm, which divided the area into a grid of boxes and counted the boxes occupied by the trajectory (e.g. Mohaghar et al., 2020). In general, complicated trajectories have greater fractal dimension relative to simple and linear trajectories. In these analyses, fractal dimension was calculated for all trajectories longer than 20 s. *Acartia tonsa* perform two types of jumps: hops and escape jumps and escapes are stronger jumps. This study differentiated hop and escape jumps by defining a threshold acceleration of 0.7 m s^{-2} , with hops corresponding to acceleration events falling below this threshold. Furthermore, coordinated jumps related to mating events were omitted from our data. Jump frequency was calculated as the number of jumps per copepod per period (s). Jump density (per unit time) was defined as the number of jumps divided by the area of a circular bin (ring) at a radial distance from the vortex axis, i.e. $A=\pi[(r+\Delta r)^2-r^2]$, where r is the radial position and $\Delta r=1\text{ mm}$ is the bin width.

Statistical analysis

Swimming kinematics in response to the Burgers vortex treatments were analyzed using a two-way ANOVA with axial strain rate (as a surrogate variable for vortex intensity) and orientation (i.e. horizontal axis or vertical axis) as independent variables. Non-normally distributed data (e.g. NGDR) were log transformed and retested for normality. ANOVA data [F -statistic, degrees of freedom (d.f.), and the significance level (P -value)] for each kinematic variable were calculated. A significance level of $P<0.05$ was used for all analyses. Linear regression was used to determine sensitivity of the mean values to the vortex intensity level analysis on variables with a significant difference in the ANOVA test. The axial strain rate parameter, a , was used as the variable to represent vortex strength in the regression analysis. Note that consistent results were obtained if instead maximum vorticity was used as the variable to represent vortex strength.

RESULTS

Acartia tonsa showed clear behavioral responses to Burgers vortex flow, and vortex intensity affected the copepod trajectory (Fig. 4). In the control treatment, copepod trajectories were generally straight and oriented predominately vertically or horizontally (Fig. 4A). As

Table 2. Sample size of trajectories for each replicate

Population	Orientation treatment	Control	Level 1	Level 2	Level 3	Level 4
Replicate 1	Horizontal	22	27	51	25	30
	Vertical	22	24	35	42	26
Replicate 2	Horizontal	32	56	41	45	28
	Vertical	42	35	37	51	35
Replicate 3	Horizontal	45	40	39	32	28
	Vertical	33	40	39	50	35

the strength of the vortex increased, the trajectories became more spiral (Fig. 4A). The percentage of spiral trajectories among the total number of trajectories increased with increasing vortex strength (Fig. 4B). Relative swimming velocity increased with vortex intensity (Fig. 5A), and the direction of swimming in the spiral trajectories was always in the flow direction, indicating that *A. tonsa* moved at elevated speed in the same direction as the swirling flow. In addition, the mean trajectory angle, with respect to the local flow direction, became smaller in higher vortex intensities (Fig. 5E) because the trajectories became increasingly directionally aligned with the rotating fluid motion. As the spiral pattern was in a plane perpendicular to the vortex axis, the mean trajectory angle with respect to the vortex axis increased with vortex intensity (Fig. 6A). Other kinematics parameters such as NGDR, fractal dimension and turn frequency were used to describe the complexity of copepod trajectories in the vortex flow, as presented below. Despite these kinematic effects, differences in proportional residence time in the vortex core were not significant across vortex intensity or orientation.

Relative swimming velocity was positively correlated with vortex intensity (regression, $t_{\text{stat}}=16.05$, $P<<0.001$, $R^2=0.9$) and in all cases the copepods swam faster than the surrounding fluid flow. In still water, the relative swimming velocity of *A. tonsa* was 0.20 ± 0.04 cm s⁻¹,

which increased to 0.45 ± 0.08 cm s⁻¹ at the highest vortex intensity (Fig. 5A). Data for the two orientation treatments were pooled as no significant difference was found for mean values in horizontal and vertical treatments (2-way ANOVA, $F_{1,29}=0.002$, $P=0.96$).

Increased turn frequency, decreased NGDR and increased fractal dimension indicated that the trajectory geometry became more convoluted with increasing vortex flow strength (Fig. 5B–D). The data showed a significant difference in turn frequency among levels of axial strain rate (2-way ANOVA, $F_{4,29}=3.612$, $P=0.023$), and no significant difference with respect to the vortex orientation (2-way ANOVA, $F_{1,29}=1.845$, $P=0.189$). Turn frequency was positively correlated with vortex strength and the mean values increased slightly from 0.138 ± 0.01 turns copepod⁻¹ s⁻¹ in the control treatment to 0.146 ± 0.02 turns copepod⁻¹ s⁻¹ in level 4 (regression, $t_{\text{stat}}=2.63$, $P=0.014$, $R^2=0.2$; Fig. 5B). Mean values of NGDR were significantly different between horizontal and vertical vortex orientations only in the vortex corresponding to the 0.09 s⁻¹ axial strain rate intensity (i.e. level 3; 2-way ANOVA, $F_{1,29}=4.83$, $P=0.04$). However, the slope of the linear regression line was not significantly different for the horizontal and vertical treatments (t -test; $t=-0.22$; $P=0.83$). There was an interactive effect between axial strain rate and vortex orientation on the mean NGDR values (2-way ANOVA, $F_{4,29}=3.10$, $P=0.039$). NGDR was negatively

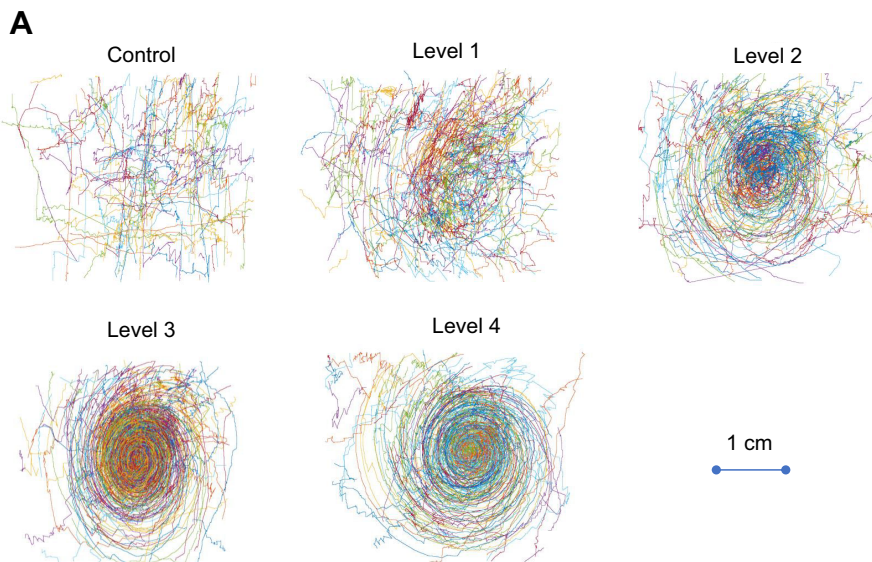
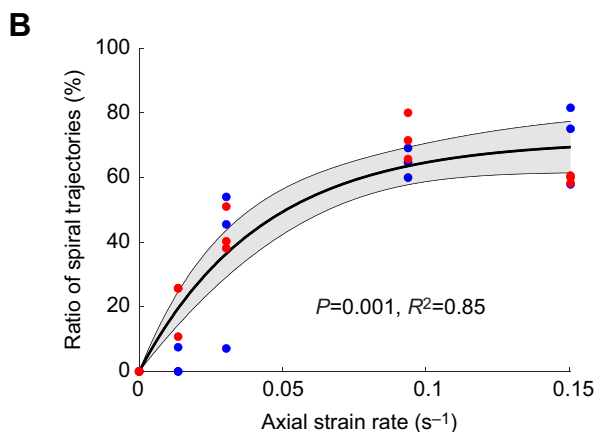


Fig. 4. Copepod trajectories. (A) Copepod trajectories in the control and the four level treatments (from the disk view) in the horizontal apparatus. The trajectory patterns change from linear and predominately vertically or horizontally directed in lower vortex strengths (control and level 1) to more spiral trajectories around the vortex axis in a stronger vortex (levels 2–4). The colors represent different trajectories. (B) Ratio of spiral trajectories to total number of trajectories reported as percentage. The percentage of copepods following a spiral trajectory (ST) was fitted to an exponential rise to a maximum (max) as a function of axial strain rate (a) as $ST = \max \times (1 - e^{-b \times a})$, where \max (71.5%) and b (23.4) were solved through numerical iteration (SigmaPlot v.11.2). Red symbols represent the vertical treatment and blue symbols represent the horizontal treatment.



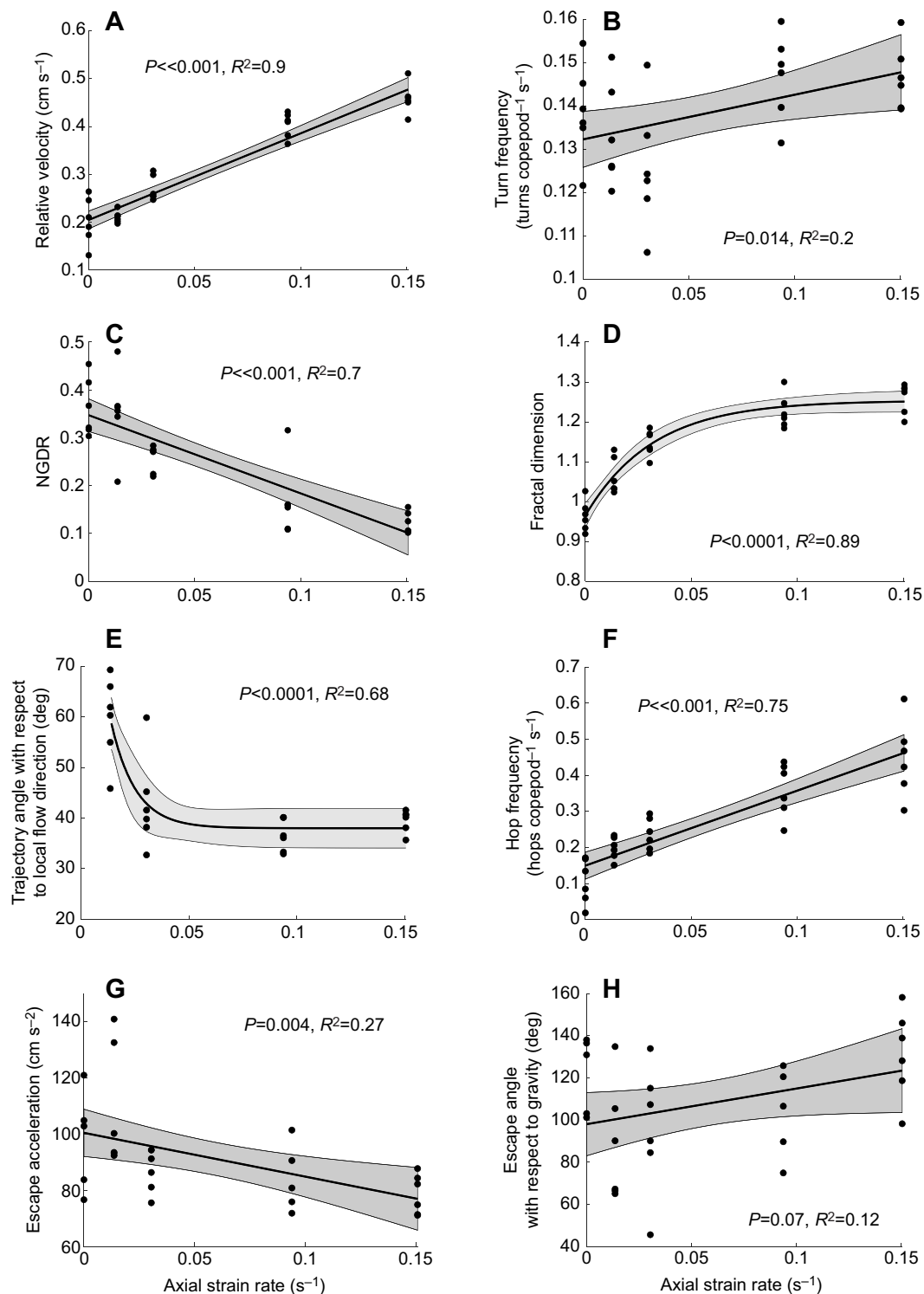


Fig. 5. Regression models of swimming kinematic parameters versus vortex axial strain rate for *Acartia tonsa* that had a significant response to vortex strength but not vortex orientation. (A) Relative swimming velocity, (B) turn frequency, (C) net-to-gross displacement ratio (NGDR), (D) fractal dimension, (E) trajectory angle with respect to the flow, (F) hop frequency, (G) escape acceleration, and (H) escape angle with respect to gravity. Data were pooled for horizontal and vertical treatments. The shaded areas show the 95% confidence interval for the parameter. The P -value and R^2 of the statistical analysis are reported for each parameter. Non-linear regression was used for D and E.

correlated with axial strain rate (Fig. 5C, i.e. the trajectories become more tortuous with increasing vortex intensity). NGDR mean values decreased from 0.41 ± 0.04 in the control treatment to 0.12 ± 0.028 in level 4 in the horizontal treatment and from 0.31 ± 0.0092 in the control treatment to 0.11 ± 0.02 in level 4 in the vertical treatment

(Fig. 5C). A non-linear regression model was used for fractal dimension ($P < 0.0001$, $R^2 = 0.89$), which showed that fractal dimension of trajectories increased with the vortex intensity, in which the mean values increased from 0.96 ± 0.04 in the control treatment to 1.26 ± 0.06 for the level 4 vortex (Fig. 5D). A small

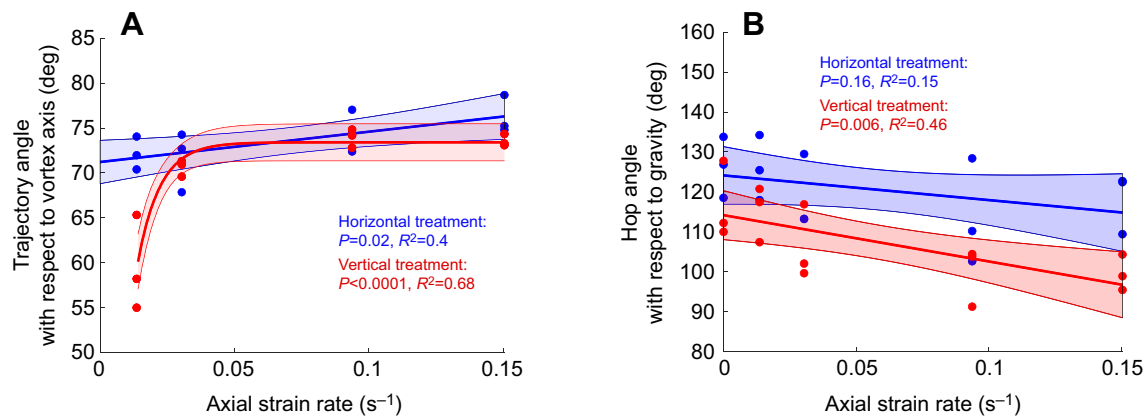


Fig. 6. Regression models of swimming kinematic parameters versus vortex axial strain rate for *A. tonsa* that had a significant response to the vortex orientation and vortex strength. (A) Trajectory angle with respect to vortex axis, and (B) hop angle with respect to gravity. Data and models are presented for horizontal (blue) and vertical (red) treatments. The shaded areas show the 95% confidence interval for the parameter. The P -value and R^2 of the statistical analysis are reported for each parameter. Non-linear regression was used for trajectory angle with respect to vortex axis for the vertical treatment.

fractal dimension value in the control treatment corresponds to linear trajectories, whereas larger values correspond to spiral trajectories. Although the mean values of fractal dimension were significantly different among levels of axial strain rate (2-way ANOVA, $F_{4,29}=48.74$, $P<0.001$), no significant response was found to the vortex orientation (2-way ANOVA, $F_{1,29}=0.656$, $P=0.427$).

The trajectory angle with respect to the local flow direction decreased exponentially with increasing axial strain rate (Fig. 5E). The mean values decreased from 60.2 ± 5.9 in level 1 to 39.5 ± 2.8 in level 4, indicating that copepods were more likely to follow the vortex flow field in a stronger vortex (regression $P<<0.0001$, $R^2=0.68$). This result further corroborates the increasing percentage of spiral trajectories with increasing vortex intensity. The trajectory angle with respect to the vortex axis also increased (i.e. became more perpendicular to the vortex axis) with increased vortex intensity (Fig. 6A). This angle was significantly different for vortex orientation (2-way ANOVA, $F_{1,23}=15.76$, $P=0.001$) and vortex strength (2-way ANOVA, $F_{3,23}=15.10$, $P<0.001$). Furthermore, there was an interaction between vortex orientation and strength (2-way ANOVA, $F_{3,23}=7.026$, $P=0.003$). In the horizontal treatment, vortex angle with respect to the vortex axis increased linearly from 72.1 ± 1.8 deg (level 1) to 76.2 ± 2.0 deg (level 4), whereas in the vertical treatment this angle increased exponentially from 59.5 ± 5.3 deg (level 1) to 73.6 ± 0.7 deg (level 4).

Hop frequency was positively correlated with vortex intensity (regression, $t_{\text{stat}}=9.15$, $P<<0.001$, $R^2=0.75$; Fig. 5F). The mean hop frequency in the control treatment was 0.10 ± 0.06 hops copepod $^{-1}$ s^{-1} and increased to 0.44 ± 0.10 hops copepod $^{-1}$ s^{-1} in level 4. Hop frequency was not dependent on vortex orientation (2-way ANOVA, $F_{1,29}=3.12$, $P=0.09$), but was significantly impacted by vortex intensity (2-way ANOVA, $F_{4,29}=21.63$, $P<0.01$).

Unlike hop frequency, no correlation was found between escape frequency and vortex strength (2-way ANOVA, $F_{4,29}=2.13$, $P=0.11$), which is perhaps due to the relatively small number of escape events. Linear regression of escape acceleration correlated negatively with vortex strength (regression, $t_{\text{stat}}=-3.11$, $P=0.004$, $R^2=0.27$; Fig. 5G). In the control treatment and level 1 treatment, copepods performed escape jumps with larger average acceleration compared with the moderate and strong vortex treatments. ANOVA indicated that the mean values were not different between the two vortex orientations (2-way ANOVA, $F_{1,27}=0.60$, $P=0.44$). Unlike the escapes, hop acceleration had no correlation with vortex strength

(2-way ANOVA, $F_{4,29}=2.59$, $P=0.30$) or vortex orientation (ANOVA, $F_{1,29}=1.10$, $P=0.06$).

Hop and escape angles with respect to gravity had no significant response to vortex strength (2-way ANOVA, $F_{3,23}=1.78$, $P=0.19$ for hop angle, and $F_{3,22}=0.77$, $P=0.52$ for escape angle) when tested within each of the vortex axis orientations. Therefore, the data from the two orientations were pooled, and hop and escape angles were tested as a function of vortex intensity. The pooled data showed significant correlation with vortex intensity for hop angle (2-way ANOVA, $F_{4,29}=3.59$, $P=0.02$) and for escape angle (2-way ANOVA, $F_{4,27}=3.38$, $P=0.03$), which indicated that the copepods' directional response relative to gravity depended on vortex intensity. Escape angle relative to gravity was not dependent on vortex orientation (2-way ANOVA, $F_{1,27}=4.38$, $P=0.051$), but hop angle with respect to gravity was significantly different for the vertical and horizontal treatments (2-way ANOVA, $F_{1,29}=17.07$, $P<0.001$). Linear regression analysis of escape angle with respect to gravity (Fig. 5H) showed no significant relationship with vortex strength (regression, $P=0.07$). The mean hop angle with respect to gravity was 110 – 135 deg in the control treatment (Fig. 6B), indicating that *A. tonsa* hopped upward. With the addition of vortex flow, the hop direction remained upward but decreased with vortex intensity (Fig. 6B). In the vertical vortex treatment, hop angle with respect to gravity decreased from 117 ± 9.7 deg in the control to 100 ± 4.5 deg in the level 4 vortex (regression, $t_{\text{stat}}=-3.29$, $P=0.006$, $R^2=0.46$). Hop angle with respect to gravity was not significantly affected by vortex intensity in the horizontal vortex treatment (regression, $t_{\text{stat}}=-1.49$, $P=0.16$, $R^2=0.15$) (Fig. 6B).

Maximum hop density occurred inside the vortex core with a radius of r_B (Fig. 7A,C). Hop density increased with vortex intensity in both vortex orientations (Fig. 7). Escapes were less frequent, and consequently escape density values were much smaller compared with hop density (Fig. 7B,D). The data also demonstrated more scatter as a result of the relatively small number of events. Nevertheless, the pattern relative to radial position was similar to the hop density with greatest escape density located in the vortex core.

DISCUSSION

Many studies have observed the behavior of copepods in turbulence. Our study investigates the interaction of individual copepods with a single vortex structure, which represents a dissipative eddy in turbulence. The Burgers vortex physical model works well to

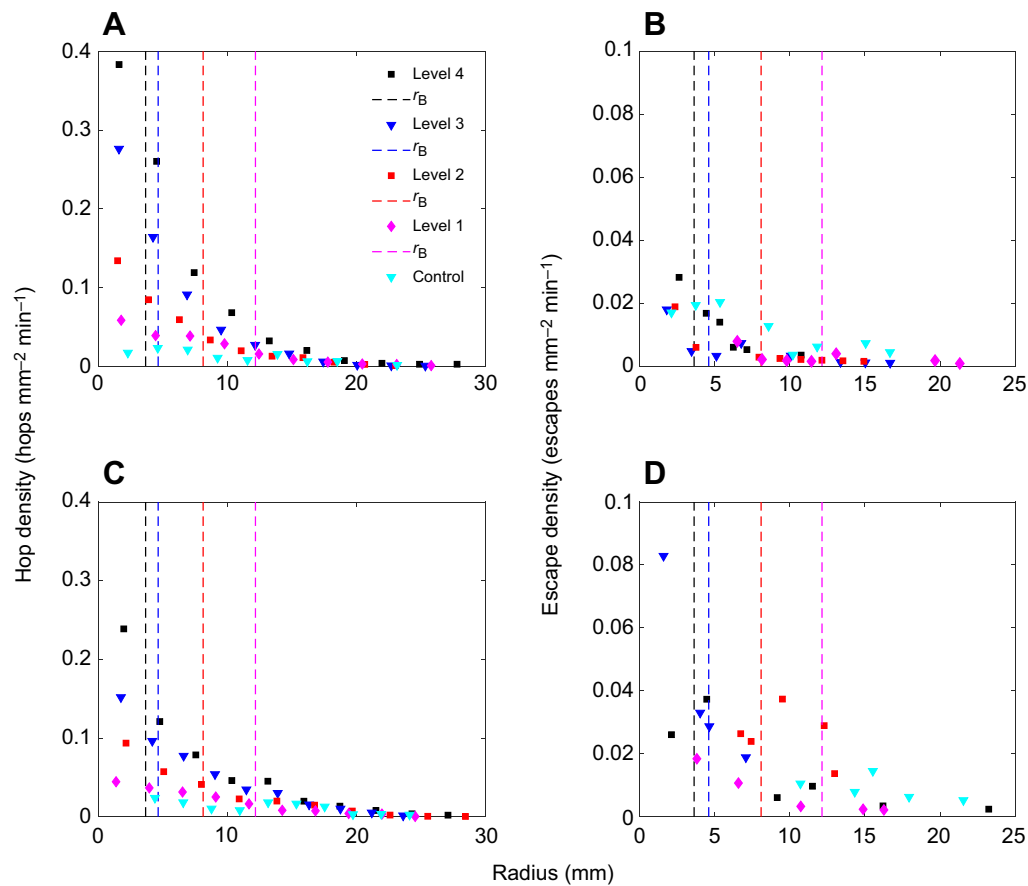


Fig. 7. Jump density as a function of distance from the vortex axis with constant bin width ($\Delta r = 1$ mm). (A) hop density for the horizontal treatment, (B) escape density for the horizontal treatment, (C) hop density for the vertical treatment, and (D) escape density for the vertical treatment. The dashed lines represent the characteristic radius of the vortex (r_B) for each level.

characterize the swimming behavior of copepods in response to small-scale dissipative eddies in turbulence. The apparatuses used in this study create stable, small vortex tubes that facilitate quantifying copepod–vortex interactions across a range of parameters. This study shows that the generated Burgers vortices in the laboratory have excellent quantitative agreement with the characteristics of typically sized turbulent eddies that copepods encounter in their habitat (Webster et al., 2004). The results in this study support the hypothesis that copepods detect and respond to the hydrodynamic cues of dissipative eddies in turbulence. By comparing the swimming kinematics of copepods in stagnant water and dissipative eddies corresponding to four turbulent intensity levels, we can gain insight into the ability of copepods to detect the hydrodynamic cues of small-scale eddies in turbulence.

Swimming speed

The findings of this study are consistent with previous observations in the level 3 Burgers vortex (Webster et al., 2015) and support the findings for *Acartia hudsonica* (Yen et al., 2008) and other copepod species (e.g. Costello et al., 1990; Marrasé et al., 1990; Saiz et al., 1992; Michalec et al., 2015) in turbulent flows. *Acartia tonsa* show increased relative swimming velocity (Fig. 5A) and hop frequency (Fig. 5F) with increasing vortex intensity. This indicates a response excited by the swirling fluid motion of the vortex. The spiral trajectories of the copepods within the vortex show that the swimming speed matches the local, surrounding fluid motion closely (Fig. 8A), indicating that *A. tonsa* are predominately being advected by the swirling vortex flow except when performing jumps or more powerful escapes (Fig. 8B). The increasing relative swimming velocity with vortex intensity is therefore explained by

the increase in hop frequency as these are the events that provide a difference between the copepod velocity and fluid velocity in the spiral trajectories. Increased swimming speed in turbulence increases the encounter rate of copepods with food, causing a higher ‘apparent food concentration’ (Rothschild and Osborn, 1988). Although turbulence causes an increased encounter rate with food items, mesocosm studies (Oviatt, 1981; Alcaraz et al., 1988) show that copepod growth rate decreased in turbulence, suggesting that greater swimming speeds and hop frequency can result in higher energetic costs. The current results suggest that the enhanced swimming behavior results from a behavior response to the hydrodynamic cues of the vortex structure itself.

Trajectory shape

The spiral swimming trajectory around the circumference of the vortex is visually striking (Fig. 4) and indicates that *A. tonsa* perceive the hydrodynamic cues and evoke behaviors that maintain it within or near the vortex. The relative swimming speeds were in the range 0.2–0.5 cm s⁻¹, whereas the largest fluid velocity for the level-4 vortex was 0.72 cm s⁻¹, which suggests that they have the ability for independent propulsion even in the strongest vortex. Yet, a large percentage of the *A. tonsa* population appear to be advected in spiral trajectories (Fig. 4B) and evoke jumps to reposition across fluid streamlines (Fig. 8). The data reveal and quantify the curved trajectories via several measures. The fraction of trajectories that exhibit a spiral shape increases with increasing vortex strength (Fig. 4B). Further, NGDR decreases (Fig. 5C) and fractal dimension of the trajectory shape increases (Fig. 5D) with increasing vortex strength, indicating more complex and loopy trajectory shapes. Turn frequency, defined as a change in heading of greater than 20 deg, is

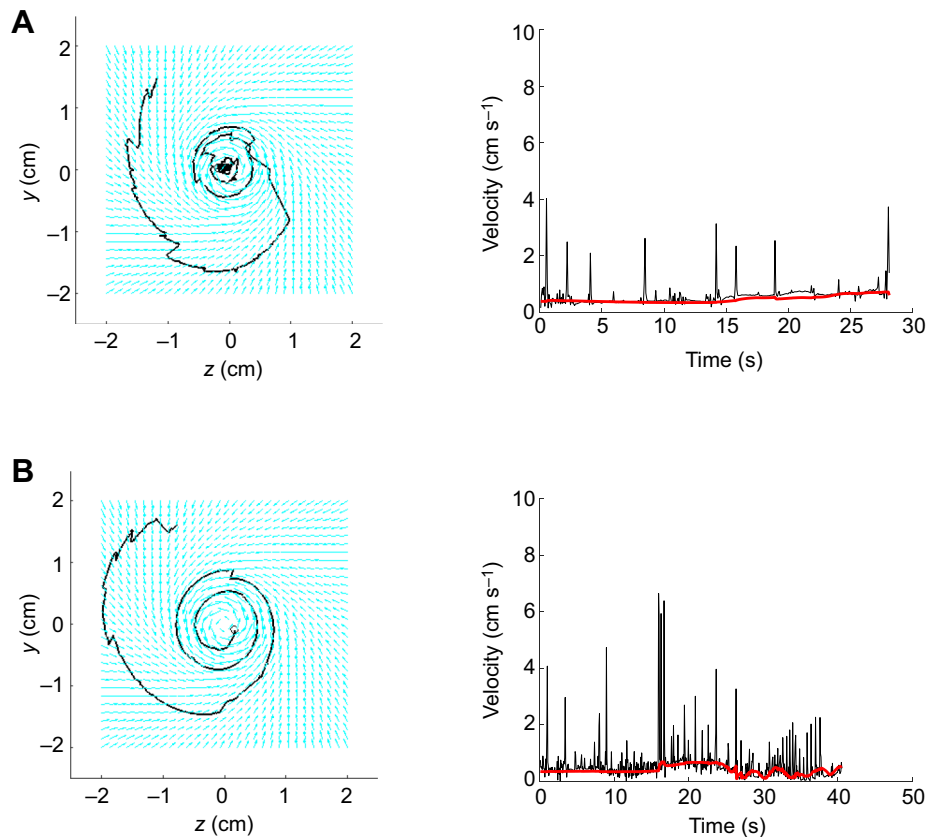


Fig. 8. Example spiral trajectories in the level 4 vortex with the corresponding time record of copepod velocity shown in black. The time record of fluid velocity at the copepod position is shown in red. (A) Infrequent hops. (B) Stronger jumps and more frequent hops and escapes. In the trajectory plots, the fluid rotation and copepod trajectory are in counterclockwise rotation.

an indicator of both the curved nature of the trajectory and the presence of angled hops (examples can be observed in Fig. 8), and it increases with vortex intensity (Fig. 5B). The spiral trajectories are always in the direction of the swirling flow motion and the angle between the copepod trajectory and the local velocity vector decreases with increasing vortex intensity (Fig. 5E). In aggregate, these trends in kinematic variables suggest that *A. tonsa* are moving purposefully with the swirling fluid motion in a Burgers vortex in a manner that enhances copepod aggregation and encounter rate with food particles and mates (Yamazaki, 1993) with minimal energy expenditure (Bartumeus et al., 2002).

Whereas the response relative to vortex intensity was significant across many kinematic parameters, the response to the vortex orientation was less significant. Copepod mechanosensors have directional sensitivity to external stimuli such as a predator (Fields, 2010; Takagi and Hartline, 2018); however, in the dissipative vortex structures, *A. tonsa* showed no difference in response to the orientation of the feature except in two kinematic parameters (shown in Fig. 6). The dependence of these parameters stands to reason as both measure an angle between the copepod motion and the relative orientation of the vortex to gravity, and one would expect the swimming style (hop–sink) of *A. tonsa* to have a fixed relationship to the direction of gravity. Hence, the dependency may result from the hop–sink motion in relation to the changing vortex orientation relative to gravity. It is suggested here that copepods are able to distinguish the hydrodynamic cues of the environment (i.e. a turbulent eddy) from a biological stimulus such as an approaching predator or prey. As turbulent eddies are ubiquitous and statistically isotropic in copepods' natural habitats, a directional response to the orientation of vortex structures may have limited ecological consequences. In contrast, directional sensitivity of copepods to

hydrodynamic signals of an approaching predator plays an important role in their survival.

Hops and escapes

Acartia tonsa execute more frequent hops in vortex treatments relative to the control and the response is positively correlated with vortex intensity level (Fig. 5F). The increased rate of hops maintains the copepods within the vortex feature. This is consistent with previous studies (e.g. Saiz and Alcaraz, 1992b; Michalec et al., 2017) that reported increased hop frequency with increased turbulence intensity. In contrast, the escape frequency relative to control did not increase with vortex intensity. Escape jumps are energetically expensive (Strickler, 1977; Alcaraz et al., 1989; Saiz and Alcaraz, 1992b) and these results show that copepods can distinguish different flow patterns to limit unnecessary escape reactions (Fields and Yen, 1997; Fields, 2000), as well as decrease escape acceleration rates with increased levels of turbulence (Fig. 5G).

The hydrodynamic cue in small-scale turbulent eddies that triggers behavioral responses in copepods remains relatively unknown. One of the advantages of the approach used in this study (i.e. a stable Burgers vortex) is that the location of the hops and escapes can be quantified relative to the spatial structure of the vortex. Furthermore, the structure of the Burgers vortex spatially separated regions of maximum shear strain rate and maximum vorticity, as described above. The location of the maximum shear strain rate is at a radial distance slightly larger than the characteristic radius, r_B . In contrast, maximum vorticity is at the center of the vortex. By comparing the spatial density of the hops and escapes at locations surrounding the vortex axis, the hydrodynamic signal that initiates the behaviors can be discerned.

Acartia tonsa showed the highest density of hops and escapes near the vortex core (Fig. 7), and the jump density decreased with radial distance from the core. These results suggest that vorticity is the hydrodynamic cue eliciting the hop and escape response in the vortex flow as the spatial patterns match (see Fig. 2B). The same conclusion was reached for *A. tonsa* based on a smaller set of results (Webster et al., 2015). It is interesting to note that the density of hops measured in the vortex exceeds the density of escape responses by more than an order of magnitude (Fig. 7). These results show that copepods do not avoid being within the vortex and the relocation hops maintain the copepods in the vortex rather than escaping from the feature. There are also asymmetries in the hop density between the horizontal and vertical orientations of the vortex. When the vortex is in the horizontal orientation, a sinking copepod moves radially within the vortex and experiences variation in the hydrodynamic signals between hops. In contrast, when the vortex is in the vertical orientation, the sinking copepod maintains the same distance from the vortex core and the hydrodynamic signal is relatively constant. As discussed in Webster et al. (2015), incorporating the axial strain rate of the Burgers vortex flow to calculate the maximum principal strain rate does not change the profile shape or the conclusion. These results support the hypothesis that copepods can distinguish different types of fluid signals in the environment. *Acartia tonsa* perform frequent, long escape jumps in response to strain rate, and not in response to vorticity, in siphon flow and other flows that simulate a suction predator (Fields and Yen, 1997; Kiørboe et al., 1999). However, the small-scale dissipative vortices present substantially different flow characteristics than used in previous studies and may cause temporary aggregations of copepods that enhance mating encounters and provide higher density patches for larger predators.

Conclusion

Metabolic rate, predator–prey encounter rate, grazing rate, egg production, swimming behavior and population dynamics of marine copepods are all affected by turbulent fluid motions. The current study concludes that the swimming behavior of *A. tonsa* is strongly influenced by small-scale eddies. It appears that swimming behavior changes in response to the dissipative-scale turbulent eddies themselves may be driving the biological and ecological effects of turbulence. This includes potentially forming aggregations as a large number of copepods swim in spiral trajectories around the vortex. Hence, the influence of these small flow structures escalates up to affect much larger scale processes.

Acknowledgements

We thank Shantanu Soumya, Yoonsoo Nam, Savannah Howard, Samantha Bennett, Dominique Howard, Agam Singh and Tara Boyd for help with digitalization of the copepod tracks. We thank Dr David Young for recording the image in Fig. 1C. Thanks also to Dr Jeannette Yen for inspiration and early discussions.

Competing interests

The authors declare no competing or financial interests.

Author contributions

Conceptualization: D.E., D.R.W., D.M.F.; Methodology: D.E., D.R.W., D.M.F.; Software: D.E.; Validation: D.E.; Formal analysis: D.E., D.R.W., D.M.F.; Resources: D.M.F.; Data curation: D.E.; Writing - original draft: D.E., D.R.W., D.M.F.; Writing - review & editing: D.E., D.R.W., D.M.F.; Supervision: D.R.W.; Project administration: D.R.W., D.M.F.; Funding acquisition: D.R.W., D.M.F.

Funding

Funding was provided by National Science Foundation grants OCE-1537284 and OCE-1537579.

Data availability

Data are available from BCO-DMO (project url <https://www.bco-dmo.org/project/653235>): doi:10.26008/1912/bco-dmo.834530.1 and doi:10.26008/1912/bco-dmo.818213.1

References

- Alcaraz, M. and Saiz, E. (1992). External energy and plankton: new insights on the role of small-scale turbulence on zooplankton ecology. *Oecol. Aquatic* **10**, 137–144.
- Alcaraz, M., Saiz, E., Marrasé, C. and Vaque, D. (1988). Effects of turbulence on the development of phytoplankton biomass and copepod populations in marine microcosms. *Mar. Ecol. Prog. Ser.* **49**, 117–125. doi:10.3354/meps049117
- Alcaraz, M., Estrada, M. and Marrasé, C. (1989). Interaction between turbulence and zooplankton in laboratory microcosms. In *Proceedings of the 21st EMBS* (ed. R. Z. Klekowski, E. Styczynska-Jurewicz and L. Falkowski), pp. 191–204. Gdansk, Poland: Polish Acad. of Sci.-Inst. of Oceanology.
- Bartumeus, F., Catalan, J., Fulco, U. L., Lyra, M. L. and Viswanathan, G. M. (2002). Optimizing the encounter rate in biological interactions: Lévy versus Brownian strategies. *Phys. Rev. Lett.* **88**, 097901. doi:10.1103/PhysRevLett.88.097901
- Browman, H. I., Yen, J., Fields, D. M., St-Pierre, J.-F. and Skiftesvik, A. B. (2011). Fine-scale observations of the predatory behaviour of the carnivorous copepod *Paraeuchaeta norvegica* and the escape responses of their ichthyoplankton prey, Atlantic cod (*Gadus morhua*). *Mar. Biol.* **158**, 2653–2660. doi:10.1007/s00227-011-1763-y
- Burgers, J. M. (1948). A mathematical model illustrating the theory of turbulence. *Adv. Appl. Mech.* **1**, 171–199. doi:10.1016/S0065-2156(08)70100-5
- Costello, J. H., Strickler, J. R., Marrasé, C., Trager, G., Zeller, R. and Freise, A. J. (1990). Grazing in a turbulent environment: Behavioral response of a calanoid copepod, *Centropages hamatus*. *Proc. Natl Acad. Sci. USA* **87**, 1648–1652. doi:10.1073/pnas.87.5.1648
- Davidson, P. A. (2015). *Turbulence: An Introduction for Scientists and Engineers*. Oxford University Press.
- Eisinga, G. E., Scarano, F., Wieneke, B. and van Oudheusden, B. W. (2006). Tomographic particle image velocimetry. *Exp. Fluids* **41**, 933–947. doi:10.1007/s00348-006-0212-z
- Fields, D. M. (2000). Characteristics of the high frequency escape reactions of *Oithona* sp. *Mar. Freshw. Behav. Physiol.* **34**, 21–35. doi:10.1080/10236240009379057
- Fields, D. M. (2010). Orientation affects the sensitivity of *Acartia tonsa* to fluid mechanical signals. *Mar. Biol.* **157**, 505–514. doi:10.1007/s00227-009-1336-5
- Fields, D. M. and Yen, J. (1997). The escape behavior of marine copepods in response to a quantifiable fluid mechanical disturbance. *J. Plankton Res.* **19**, 1289–1304. doi:10.1093/plankt/19.9.1289
- Fields, D. M. and Yen, J. (2002). Fluid mechanosensory stimulation of behaviour from a planktonic marine copepod *Euchaeta rimana* Bradford. *J. Plankton Res.* **24**, 747–755. doi:10.1093/plankt/24.8.747
- Fields, D. M., Shema, S. D., Browman, H. I., Browne, T. Q. and Skiftesvik, A. B. (2012). Light primes the escape response of the calanoid copepod, *Calanus finmarchicus*. *PLoS ONE* **7**, e39594. doi:10.1371/journal.pone.0039594
- Granata, T. C. and Dickey, T. D. (1991). The fluid mechanics of copepod feeding in a turbulent flow: a theoretical approach. *Prog. Oceanogr.* **26**, 243–261. doi:10.1016/0079-6611(91)90003-5
- Haury, L. R., Yamazaki, H. and Itsweire, E. C. (1990). Effects of turbulent shear flow on zooplankton distribution. *Deep Sea Res. A* **37**, 447–461. doi:10.1016/0198-0149(90)90019-R
- Heath, M. R., Henderson, E. W. and Baird, D. L. (1988). Vertical distribution of herring larvae in relation to physical mixing and illumination. *Mar. Ecol. Prog. Ser.* **47**, 211–228. doi:10.3354/meps047211
- Hedrick, T. L. (2008). Software techniques for two- and three-dimensional kinematic measurements of biological and biomimetic systems. *Bioinspir. Biomim.* **3**, 034001. doi:10.1088/1748-3182/3/3/034001
- Incze, L. S., Hebert, D., Wolff, N., Oakey, N. and Dye, D. (2001). Changes in copepod distributions associated with increased turbulence from wind stress. *Mar. Ecol. Prog. Ser.* **213**, 229–240. doi:10.3354/meps213229
- Jumars, P. A., Trowbridge, J. H., Boss, E. and Karp-Boss, L. (2009). Turbulence-plankton interactions: a new cartoon. *Mar. Ecol. Evol. Perspect.* **30**, 133–150. doi:10.1111/j.1439-0485.2009.00288.x
- Kiørboe, T. and Saiz, E. (1995). Planktivorous feeding in calm and turbulent environments, with emphasis on copepods. *Mar. Ecol. Prog. Ser.* **122**, 135–145. doi:10.3354/meps122135
- Kiørboe, T., Saiz, E. and Visser, A. (1999). Hydrodynamic signal perception in the copepod *Acartia tonsa*. *Mar. Ecol. Prog. Ser.* **179**, 97–111. doi:10.3354/meps179097
- Lagadeuc, Y., Bouté, M. and Dodson, J. J. (1997). Effect of vertical mixing on the vertical distribution of copepods in coastal waters. *J. Plankton Res.* **19**, 1183–1204. doi:10.1093/plankt/19.9.1183
- Mackas, D. L., Sefton, H., Miller, C. B. and Raich, A. (1993). Vertical habitat partitioning by large calanoid copepods in the oceanic subarctic Pacific during Spring. *Prog. Oceanogr.* **32**, 259–294. doi:10.1016/0079-6611(93)90017-8
- Manning, C. A. and Bucklin, A. (2005). Multivariate analysis of the copepod community of near-shore waters in the western Gulf of Maine. *Mar. Ecol. Prog. Ser.* **292**, 233–249. doi:10.3354/meps292233
- Marrasé, C., Costello, J. H., Granata, T. and Strickler, J. R. (1990). Grazing in a turbulent environment: Energy dissipation, encounter rates, and efficacy of

- feeding currents in *Centropages hamatus*. *Proc. Natl. Acad. Sci. USA* **87**, 1653–1657. doi:10.1073/pnas.87.5.1653
- Michalec, F.-G., Souissi, S. and Holzner, M.** (2015). Turbulence triggers vigorous swimming but hinders motion strategy in planktonic copepods. *J. R. Soc. Interface* **12**, 20150158. doi:10.1098/rsif.2015.0158
- Michalec, F.-G., Fouxon, I., Souissi, S. and Holzner, M.** (2017). Zooplankton can actively adjust their motility to turbulent flow. *Proc. Natl. Acad. Sci. USA* **114**, E11199–E11207. doi:10.1073/pnas.1708888114
- Mohaghar, M., Jung, S., Haas, K. A. and Webster, D. R.** (2020). Copepod behavior responses around internal waves. *Front. Mar. Sci.* **7**, 331. doi:10.3389/fmars.2020.00331
- Murphy, D. W., Webster, D. R. and Yen, J.** (2012). A high-speed tomographic PIV system for measuring zooplanktonic flow. *Limnol. Oceanogr.* **10**, 1096–1112. doi:10.4319/lom.2012.10.1096
- Oviatt, C. A.** (1981). Effects of different mixing schedules on phytoplankton, zooplankton and nutrients in marine microcosms. *Mar. Ecol. Prog. Ser.* **4**, 57–67. doi:10.3354/meps004057
- Rothschild, B. J. and Osborn, T. R.** (1988). Small-scale turbulence and plankton contact rates. *J. Plankton Res.* **10**, 465–474. doi:10.1093/plankt/10.3.465
- Saffman, P. G.** (1997). Vortex models of isotropic turbulence. *Phil. Trans. R. Soc. Lond. A* **355**, 1949–1956. doi:10.1098/rsta.1997.0097
- Saiz, E. and Alcaraz, M.** (1992a). Enhanced excretion rates induced by small-scale turbulence in *Acartia* (Copepoda: Calanoida). *J. Plankton Res.* **14**, 681–689. doi:10.1093/plankt/14.5.681
- Saiz, E. and Alcaraz, M.** (1992b). Free-swimming behaviour of *Acartia clausi* (Copepoda: Calanoida) under turbulent water movement. *Mar. Ecol. Prog. Ser.* **80**, 229–236. doi:10.3354/meps080229
- Saiz, E. and Kiørboe, T.** (1995). Predatory and suspension feeding of the copepod *Acartia tonsa* in turbulent environments. *Mar. Ecol. Prog. Ser.* **122**, 147–158. doi:10.3354/meps122147
- Saiz, E., Alcaraz, M. and Paffenhöfer, G.-A.** (1992). Effects of small-scale turbulence on feeding rate and gross-growth efficiency of three *Acartia* species (Copepoda: Calanoida). *J. Plankton Res.* **14**, 1085–1097. doi:10.1093/plankt/14.8.1085
- Strickler, J. R.** (1977). Observation of swimming performances of planktonic copepods. *Limnol. Oceanogr.* **22**, 165–170. doi:10.4319/lo.1977.22.1.0165
- Takagi, D. and Hartline, D. K.** (2018). Directional hydrodynamic sensing by free-swimming organisms. *Bull. Math. Biol.* **80**, 215–227. doi:10.1007/s11538-017-0368-0
- Tiselius, P.** (1992). Behavior of *Acartia tonsa* in patchy food environments. *Limnol. Oceanogr.* **37**, 1640–1651. doi:10.4319/lo.1992.37.8.1640
- Vincent, A. and Meneguzzi, M.** (1991). The spatial structure and statistical properties of homogeneous turbulence. *J. Fluid Mech.* **225**, 1–20. doi:10.1017/S0022112091001957
- Visser, A. W., Saito, H., Saiz, E. and Kiørboe, T.** (2001). Observations of copepod feeding and vertical distribution under natural turbulent conditions in the North Sea. *Mar. Biol.* **138**, 1011–1019. doi:10.1007/s002270000520
- Webster, D. R. and Young, D. L.** (2015). A laboratory realization of the Burgers' vortex cartoon of turbulence-plankton interactions. *Limnol. Oceanogr.* **13**, 92–102. doi:10.1002/lom3.10010
- Webster, D. R., Brathwaite, A. and Yen, J.** (2004). A novel laboratory apparatus for simulating isotropic oceanic turbulence at low Reynolds number. *Limnol. Oceanogr.* **2**, 1–12. doi:10.4319/lom.2004.2.1
- Webster, D. R., Young, D. L. and Yen, J.** (2015). Copepods' response to Burgers' vortex: deconstructing interactions of copepods with turbulence. *Integr. Comp. Biol.* **55**, 706–718. doi:10.1093/icb/icc054
- Woodson, C. B., Webster, D. R. and True, A. C.** (2014). Copepod behavior: oceanographic cues, distributions, and trophic interactions. In *Copepods: Diversity, Habitat, and Behavior* (ed. L. Seuront), pp. 215–253. Hauppauge, NY: Nova Publishers.
- Yamazaki, H.** (1993). Lagrangian study of planktonic organisms: perspectives. *Bull. Mar. Sci.* **53**, 265–278.
- Yen, J., Lenz, P. H., Gassie, D. V. and Hartline, D. K.** (1992). Mechanoreception in marine copepods: Electrophysiological studies on the first antennae. *J. Plankton Res.* **14**, 495–512. doi:10.1093/plankt/14.4.495
- Yen, J., Rasberry, K. D. and Webster, D. R.** (2008). Quantifying copepod kinematics in a laboratory turbulence apparatus. *J. Mar. Syst.* **69**, 283–294. doi:10.1016/j.jmarsys.2006.02.014